A new regional, mid-Holocene palaeoprecipitation signal of the Asian Summer Monsoon

D. Strong[1,2], R. Flecker[1], P.J. Valdes[1], I.P. Wilkinson[3], J.G. Rees[3], K. Michaelides[1], Y.Q. Zong[4], J.M. Lloyd[5], F.L. Yu[6] and R.D. Pancost[2]

Addresses: 1. School of Geographical Sciences, University of Bristol, University Road, Bristol BS8 1SS, UK

2. Organic Geochemistry Unit, Bristol Biogeochemistry Research Centre and The Cabot Institute, School of Chemistry, University of Bristol, Cantocks Close, Bristol BS8 1TS, UK

3. British Geological Survey, Kingsley Dunham Centre, Keyworth, Nottingham NG12 5GG, UK

4. Department of Earth Sciences, University of Hong Kong, James Lee Sciences Building, Pokfulam Road, Hong Kong SAR, China

5. Department of Geography, University of Durham, South Road, Durham DH1 3LE, UK

6. Earth Observatory of Singapore, Nanyang Technological University, 50 Nanyang Avenue, Block N2-01a-15, Singapore 639798.

Corresponding author: Dr Rachel Flecker, School of Geographical Sciences, University of Bristol, University Road, Bristol BS8 1SS, UK. Tel: +44 (0)117 3317267. E-mail: r.flecker@bristol.ac.uk

Classification: PHYSICAL SCIENCES: Earth, Atmospheric, and Planetary Science

Abstract

The Dongge Cave speleothem $\delta^{18}O$ record, which lies in the Pearl River basin (China), has been interpreted as recording a regional decline in Asian Summer Monsoon precipitation over the last 6.5 kyrs. The same overall trend is seen in the bulk sedimentary organic $\delta^{13}C_{org}$ record from a core in the Pearl River Estuary. However, the two records differ in detail and the regional nature of the Dongge palaeoprecipitation signal has therefore been questioned. Our study re-evaluates both records by constructing, for the same estuarine core, biomarker and compound-specific $\delta^{13}C$ records, which have better constrained terrestrial and marine end members than $\delta^{13}C_{org}$, providing additional insights into the evolution of the Asian Summer Monsoon.

The Branched Isoprenoidal Tetraether (BIT) index reflects the ratio of soil versus marine organic matter. The BIT record from the estuarine core co-varies with the Dongge Cave $\delta^{18}O$ record suggesting the two share a common control which is likely to be driven by regional climate. By contrast, the sterols, *n*-alcohols and *n*-fatty acid ratios show the same overall trend as Dongge, but parallel the $\delta^{13}C_{org}$ record's variability between 6.5-2 kyrs indicating a partial decoupling between soil and land-plant organic matter fluxes in the Pearl River Basin. There is clear divergence between the biomarker and $^{13}C_{org}$ records from 2 kyrs to present. Analysis of the leaf wax $\delta^{13}C$ suggests that this results from an abrupt change in vegetation probably resulting from local, anthropogenic cultivation two thousand years ago.

The basin scale of these estuarine records equates to up to 15 grid cells in typical Earth System Models used for simulating global climate. This permits comparison of Palaeoclimate Model Intercomparison Project simulations of the mid-Holocene with spatially equivalent data relating to the Summer Asian Monsoon, for the first time.

1. Introduction

Changes in the intensity of the Asian Summer Monsoon may have contributed to the historical collapse of the Tang, Qin and Shang dynasties in China (Shi et al., 1994; Yancheva et al., 2007; Zhang et al., 2008). Today, China is occupied by approximately half the global human population. There is therefore an urgent need for accurate reconstructions and predictions of monsoon variability on annual to centennial timescales (Webster et al., 1998). Reconstructing past changes in the monsoon contributes to understanding its behaviour which

is a prerequisite for accurate modelling and prediction. This study presents new evidence of the influence of the Asian Summer Monsoon on the Pearl River basin (Fig. 1) over the last six thousand years and uses these data to test model simulations of the Asian Summer Monsoon in the mid-Holocene.

Previous reconstructions of mid- to late-Holocene Asian Summer Monsoon intensity have largely relied on palaeoprecipitation proxy records from lakes (e.g. Fang, 1991; Huang et al., 1997), pollen and vegetation assemblages (e.g. An et al., 2004; Liu and Huang, 2005), cave speleothems (e.g. Dong et al., 2010; Wang et al., 2005; Zhang et al., 2004) and organic matter flux (Yu et al., 2012; Zong et al., 2006; Zong et al., 2010). Overall, these datasets indicate a general decline in precipitation across Asia from 6.5 ka to present. However, there are noticeable discrepancies in the timing and pattern of precipitation change between different records. For example, although high-resolution cave speleothem records from the Asian Summer Monsoon region (Dong et al., 2010; Wang et al., 2005; Zhang et al., 2004) have conventionally been interpreted as indicating decreasing monsoon intensity during the mid to late Holocene, the exact timing and rate of the decline in palaeoprecipitation varies between many of the speleothem-based proxy records. The Sanbao Cave in China (Fig. 1) records a gradual decline from 6.5 ka to present (Dong et al., 2010), whereas records from Xiangshui (Zhang et al., 2004) and Dongge (Wang et al., 2005) record a gradual decline from 6.5 ka to 3 ka, followed by relatively stable precipitation from 3 ka to present (Fig. 2). Lake records in central and southern China document a period of lower precipitation levels at 4-5 ka (Fang, 1991) which is not seen in the other datasets, and pollen assemblages record an abrupt reduction in Asian Summer Monsoon moisture flux to the Loess Plateau at 6.3 ka (An et al., 2004) which is also not mirrored elsewhere. There are two possible causes for these apparent discrepancies: either, one or more of the proxies do not reflect quantity of rainfall e.g. it has been suggested that the Chinese speleothem $\delta^{18}O$ records are responding to rainfall source rather than rainfall amount (Maher and Tompson, 2012), or, since each proxy monitors a signal on a relatively local scale of tens of square kilometres, the records are susceptible to local influences overprinting the regional signal.

One of the uses of proxy records is the validation of global-scale Earth System Models which provide insight into future climate behaviour. Unfortunately however, the size of grid cells in these models is usually significantly larger than the scale recorded by lake, cave and

vegetation-based systems (Lunt et al., 2008; Markwick and Valdes, 2004). Because of this scale disparity, robust validation is problematic. Modelling studies that have focussed on the East Asian Monsoon and sought to compare output with proxy data are no exception (e.g. Tao et al., 2010). Records, which capture climate variables such as temperature and precipitation on a spatial-scale comparable to, or larger than the model's grid squares (typically 1000s km^2), would permit more robust model-data comparison and hence decrease some of the uncertainties associated with climate-model predictions. Large river drainage basins are scale equivalent to one or more model grid cells (Fig. 1), but to use them in this capacity assumes that the precipitation signal is integrated across the basin and recorded in the estuarine geological archive. This assumption can be made because large basin areas tend to capture the regional precipitation signal, even though they are typically more complex and exhibit higher hydrological variability than small ones. Large basins are, therefore, better integrators of the regional climate signal over the longer term (e.g. Weijers et al., 2009).

Previous reconstructions of relative terrestrial sediment transport to the Pearl River Estuary using bulk organic carbon isotopes (Yu et al., 2012; Yu, 2009; Zong et al., 2006; Zong et al., 2010) have attempted to use this approach to provide a regional signal. These $\delta^{13}C_{org}$ records show a general increasing trend with time (Fig. 2), which is thought to result from a decrease in the ratio of ^{13}C-depleted terrestrial organic matter relative to ^{13}C-enriched marine organic matter. Consequently, the $\delta^{13}C_{org}$ record has been interpreted as indicating a decline in monsoonal rainfall with time. The $\delta^{13}C_{org}$ trend is largely consistent with the trend in the Dongge $\delta^{18}O$ cave record which lies within the Pearl River basin (Fig. 1), but in detail there are differences between the two records (Fig. 2). These disparities have been attributed to a difference in basin size with the $\delta^{13}C_{org}$ reflecting a more regional climate signal relative to the more localised Dongge signal (Yu et al., 2012; Fig. 1). However, the marine and terrestrial $\delta^{13}C$ end-members can be ambiguous, and a shift in basin vegetation, for example from C_3 to C_4 grasses, could contribute to a significant change in the $\delta^{13}C$ value of the terrestrial end member and alter the $\delta^{13}C_{org}$ of the estuarine sediment. Therefore, the differences between the Dongge and estuarine bulk $\delta^{13}C$ record could result from changes in the nature of the terrestrial and/or marine organic matter supplied to the Pearl River estuary rather than a difference in geographical scale of the precipitation signal recorded.

Our study addresses this ambiguity by constructing biomarker distribution records that have different end-member uncertainties from bulk organic $\delta^{13}C$ values, as well as compound-specific $\delta^{13}C$ records that allow a direct examination of the terrestrial end-member used in interpretation of the bulk organic $\delta^{13}C$ values. These are used both to test whether deviations between the $\delta^{13}C_{org}$ record and the Dongge speleothem result from changes in vegetation $\delta^{13}C$ values that influence the $\delta^{13}C_{org}$, and to develop new records for changes in the sedimentary inputs to the Pearl River Estuary. Our aim is to use these new data to establish the regional record of monsoon precipitation over the last 6.5 ka and to compare that with existing Earth System Model simulations of the Mid-Holocene from the Palaeoclimate Model Intercomparison Project (PMIP2).

2. Materials and methods

With an area of over 400,000 km^2, the Pearl River basin is the second largest drainage basin in China after the Yangtze. Over 90% of the basin's mean annual precipitation occurs during the summer monsoon period (China Meteorological Data Sharing Service System; CMDSSS, 2011) and it drains into the South China Sea through the Pearl River Estuary (Fig. 1). Fluvial sediment influx to the estuary occurs predominantly during the wet season, between April and October (Cai et al., 2004) and sedimentation rates at the estuary mouth around Hong Kong have been shown to be substantially lower than in the upper estuary shoals (Li et al., 1991; Owen, 2005; Zong et al., 2009). Measurements of monthly water discharge and sediment load over four decades at three stations on the Pearl River show a linear relationship (Zhang et al., 2008) suggesting that Pearl River Basin is transport limited. However, although we can assume that over the long term, regional precipitation changes affect the supply of sediment to the estuary, we do not make assumptions about the sources of this sediment (i.e. from erosion of highlands or lowland floodplains).

Except for occasional erosion and redeposition by storms and typhoons, normal estuarine sediments are well preserved in the Pearl River Estuary (Yu, 2009) which experiences a small tidal range (0.86-1.6m, Owen, 2005). Since the Last Glacial Maximum, sea level has steadily risen in the South China Sea, flooding the current estuarine area by ~7 ka (Zong, 2004). However from 6.5 ka to present, sea level in this area, has been relatively stable (Yu et al., 2012; Zong, 2004) and significant delta progradation has occurred (Zong et al., 2009).

Fifty, approximately evenly spaced samples were taken from the top 10 m of a sediment core (HKUV-1, Fig. 1b) located on the pro-delta, close to the delta toe (22º17'10"N, 113º51'49"E) in a water depth of -9.00 m Yellow Sea Datum.

^{14}C-dating was carried out on foraminiferal calcite and well-preserved bivalves from seven levels in the top 10 m of core material (Yu et al., 2012; Yu, 2009; Supplementary Information). The age range of these samples was between 0 - 6,384 YBP and the data document a clear decline in sedimentation rate with time. The average sedimentation rate for this section of the core is ~1.57 mm yr^{-1}, so each 1-cm thick subsample represents approximately a 6.4-yr mean record (Yu et al., 2012; Yu, 2009).

This study focuses on four biomarker-based ratios: the Branched Isoprenoidal Tetraether (BIT) index; the ratio of $\Sigma C_{26\text{-}34}/(\Sigma C_{26\text{-}34}+\Sigma C_{16+18})$ *n*-fatty acids; an analogous ratio for *n*-alcohols; and the ΣC_{29}-steroids/(ΣC_{29}-steroids + brassicasterol) ratio. These ratios and their concentrations, details of the extraction and fractionation procedure along with the instrumental analysis are described in the Supplementary Information and Tables SI-1 to SI-5 inclusive. The BIT index has been previously used as a proxy for relative terrestrial organic matter input into the marine environment (Hopmans et al., 2004) and is calculated as in Equation 1.

$$BIT = (I+II+III) / (I+II+III+IV) \quad 1$$

It is a ratio of branched GDGTs (compounds I-III in Hopmans et al., 2004) sourced from putative terrestrial bacteria (Weijers et al., 2007) against crenarchaeol (IV in Hopmans et al., 2004), a GDGT derived from marine (pelagic) ammonia-oxidising Thaumarchaeota (Schouten et al., 2000). The biomarker end-members of the BIT index are consequently from relatively narrow and well defined marine or terrestrial origins.

By contrast,the *n*-fatty acid, *n*-alcohol and sterol ratios have numerators ($C_{26\text{-}34}$ *n*-fatty acids, $C_{26\text{-}34}$ *n*-alcohols and C_{29} steroids) which encompass a range of higher plant vegetation (Eglinton and Hamilton, 1967; Freeman and Colarusso, 2001), but can also derive from some aquatic algal sources (e.g. Volkman, 1986; Volkman et al., 1999; Volkman et al., 1998). Similarly, the aquatic denominators of these ratios (C_{16+18} *n*-fatty acids, C_{16+18} *n*-alcohols and brassicasterol respectively) can derive from a range of water column phytoplankton and

sedimentary bacteria as well as soil bacteria and higher plants. These biomarker ratios, therefore, capture a broad range of the terrestrial and marine inputs, providing an additional but complex constraint on the nature and origin of OM being delivered to the Pear River Estuary over time.

3. Results

All of the sediments contain a diverse array of aquatic and terrigenous biomarkers (supplementary information). The polar fractions are dominated by a homologous series (C_{12}-C_{34}) of *n*-alcohols, the most abundant of which are the $C_{22\text{-}30}$ homologues, and a range of $C_{27\text{-}30}$ sterols. They all also contain branched and isoprenoid glycerol dialkyl glycerol tetraethers (GDGTs). All of the core sediments contain an acid fraction that is dominated by a homologous series (C_{12}-C_{34}) of straight chain *n*-fatty acids. These allow calculation of a range of biomarker parameters indicative of organic matter source. Intriguingly, the apolar (saturated hydrocarbon) fractions are dominated by an unresolved complex mixture, as observed in modern Pearl River Estuary sediments (Strong et al., 2012), precluding analysis of the *n*-alkane distributions.

3.1 BIT indices

BIT indices from these sediments vary from 0.76 to 0.54 (Fig. 3a; Table SI-1) which is within the range of values displayed by modern sediments (0.98 to 0.23) across the entire estuary from the Pearl River mouth to the South China Sea (Fig. 1b; Strong et al., 2012). The core's BIT indices decrease from 6 ka to the present, with the major decline occurring between about 5.5-2.5 ka (Fig. 3a). This decline in the BIT index record closely parallels the Dongge Cave $\delta^{18}O$ speleothem record (Fig. 3a). Values from 2 ka to present are low (0.55-0.60), but at 1.2 ka there is a single data point that records a significantly lower BIT index (Table SI-1). This sample is from a region of the core that has been previously attributed to a marine storm event associated with significant marine deposition (Yu, 2009; Zong et al., 2010).

The MBT and CBT indices (methyl branched and cyclised branched tetraethers; Weijers et al., 2007) arise from the degree of branching and cyclisation of soil bacterial GDGTs, and together have been shown to reflect the mean annual air temperature in which the branched GDGTs were synthesised (Weijers et al., 2007; Supplementary Information). The original calibration of Weijers et al. (2007) has recently been updated with a much larger dataset

(Peterse et al., 2012), and it is that calibration we use here (although differences are <2 ºC). Caution is necessary when interpreting MBT-CBT derived mean annual air temperatures since there is a large (±5 ºC) standard error in the global calibration (Peterse et al., 2012; Weijers et al., 2007), and several studies have shown that regional or local calibrations can systematically differ from the global calibration by as much as 5 °C (Bendle et al., 2010; Sinninghe-Damsté et al., 2008; Tierney and Russell, 2009; Tierney et al., 2010). Nonetheless, MBT and CBT indices exhibit little variability in HKUV-1 (Fig. 4; Table SI-1), and all MBT-CBT derived mean annual air temperatures throughout the core are within error of the range observed in modern estuarine sediments (Strong et al., 2012). This may suggest that there has been no significant temperature change in the Pearl River basin since 6.5 ka. However, the consistent temperature may also reflect the homogenisation effect of sediment storage within the basin.

3.2 *n*-alcohol-, *n*-fatty acid- and sterol-based ratios

Concentrations of *n*-alcohols in the core sediments vary from 1.7 to 58.5 μg g^{-1}, (Table SI-2) consistent with concentrations found in sediments from the modern estuary (Hu et al., 2009; Strong et al., 2012). A series of ratios were used to explore the distributions of these biomarkers: the ratio of high- to low-molecular-weight homologues (e.g. Bourbonniere and Meyers, 1996; Fabbri et al., 2005), carbon preference index (CPIs; McCaffrey et al., 1991) and average chain lengths (ACLs; Gagosian and Peltzer, 1986) of the high molecular weight (HMW) *n*-alcohols ($C_{26\text{-}34}$). The equations used for calculation of CPI and ACL are as follows:

$$CPI = 1.5*([C_{26}]+[C_{28}]+[C_{30}]+[C_{32}]+[C_{34}])/([C_{25}]+[C_{27}]+[C_{29}]+[C_{31}]+[C_{33}]) \quad (2)$$

$$ACL = ([C_{25}]*25 + [C_{26}]*26 + [C_{27}]*27\ldots + [C_{34}]*34)/[\Sigma C_{25\text{-}34}] \quad (3)$$

and their values are shown in Table SI-3. Neither the CPIs nor ACLs exhibit systematic down-core trends. However, there is an overall, irregular decrease in the HMW/LMW+HMW *n*-alcohol ratio (where LMW stands for low molecular weight) from 6.5 ka to present, from values >0.8 at 6.5 ka to values <0.6 at 0 ka (Fig. 3b). The *n*-alcohol data show far more variability than the gradual decline seen in the BIT record, with peaks at 6.5 and 4.5 ka (Fig. 3b). The *n*-alcohol values occurring between 2-3.5 ka are generally high, but are distinctly more variable than those of the earlier section of core where the data chart systematic rising and falling trends (Fig. 3b). Sediments from the upper part of the core from 2 ka have consistently low values (Fig. 3b).

The C_{27-29} sterols and stanols occur in all samples in concentrations similar to those of the *n*-alcohols (2.3-14μg g^{-1}; Table SI-4). The C_{29} sterols exhibit large variations in concentration throughout the core, with peaks occurring at 5.0 ka and 2.6 ka (Fig. SI-3c); sediments from 6.5 ka to 2 ka have high, but variable concentrations, whereas sediments deposited after 2 ka have concentrations that are all relatively low. The variability of the (C_{29} sterols)/(brassicasterol+C_{29} sterols) ratio in the core is strikingly similar to that of the *n*-alcohol parameter (Fig. 3b).

Concentrations of *n*-fatty acids range from 5-92 μg g^{-1} (Table SI-5). The predominant *n*-fatty acids are C_{22-30} homologues with an even-over-odd preference (CPI 10.4-12.9, calculated as for the *n*-alcohols), typical of sediments containing terrigenous, higher plant-derived lipids (Collister et al., 1994; Eglinton and Hamilton, 1967; McCaffrey et al., 1991). These CPIs are significantly >1, also suggesting that the acid fraction is not derived from the petroleum source which dominates the saturated hydrocarbon fractions (Freeman and Colarusso, 2001; Nishimura and Baker, 1986). The CPIs exhibit no systematic temporal variability, which indicates both that they have undergone no significant degradation over time and that these epicuticular leaf waxes were not retained for lengthy periods in terrestrial soil (Hedges and Oades, 1997). The HMW (C_{26-34}) ACLs range from 27.3 to 29.0. Again this is typical of higher plant leaf waxes and is within the range of values recorded in the modern estuary (Strong et al., 2012). Widely-sourced LMW C_{16} and C_{18} fatty acids (Eglinton and Hamilton, 1967; Fang et al., 2002; Jones, 1969; Volkman et al., 1998) are also present in all core samples. These LMW fatty acids have previously been utilised as marine-source biomarkers in coastal settings (Gogou and Stephanou, 2004). C_{22-30} diacids are also present throughout the core but were not quantified. Temporal variation is expressed by the HMW/(LMW+HMW) ratios (Fig. 3b), and again the pattern clearly parallels that seen in the corresponding sterol and *n*-alcohol ratios.

In summary, all ratios are generally low (and largely consistent with modern values) in sediments deposited from 2 ka to present (Fig. 3b). The records from samples older than 2 ka are highly variable with peak values at ~6 ka and ~4.5 ka, minima around 5.5 and 3 ka and an interval of high variability between 3-2 ka. All of the biomarker records record an anomalously low ratio for the sample at 1.2 ka (Fig. 3; Table SI-1) thought to have been deposited by a marine storm event (Yu, 2009; Zong et al., 2010). The concentrations and mass accumulation rates of the putative plant biomarkers (i.e. the numerators of all three

ratios) exhibit similar trends, albeit with considerably greater scatter than exhibited by the ratios (Figure SI-4); thus, they confirm that the ratios are generally recording changing terrestrial OM inputs. However, they contrast with the more systematic decline seen in the BIT index from ~5.5-2.5 ka (Fig. 3a).

3.3 Leaf wax $\delta^{13}C$ values

Stable carbon isotope ratios of the highest concentration HMW fatty acids, C_{26}, C_{28} and C_{30} from the core samples have rather low $\delta^{13}C$ values (-37 to -27‰; Table SI-1; Fig. SI-5). The summed, mass-weighted $C_{26\text{-}34}$ *n*-fatty acid $\delta^{13}C$ values of the HKUV-1 core are plotted in Fig. 5b. All HMW fatty acid $\delta^{13}C$ values are between -28.5 to -35‰, spanning the range represented by C_3 plants or mixed C_3-C_4 communities (Lockheart et al., 1997). The $\delta^{13}C$ values obtained for older sediments are low (-31 to -35 ‰) relative to younger samples, with an abrupt shift to higher $\delta^{13}C$ values (-28 to -31 ‰) occurring at ~2 ka (Fig. 5b).

4. Discussion

The controls on sediment delivery to estuaries are diverse and complex. They include precipitation intensity and seasonality, sea level, tidal effects and anthropogenic influences. Where other controls remain static and sediment transport rather than sediment supply is the limiting factor, increased precipitation typically leads to higher sediment delivery to the estuary. As a consequence of the size of the basin and lowland sediment storage, there is a time lag between precipitation-driven erosion events in the highlands and the delivery of that eroded sediment to the estuary. This time lag tends to increase with basin size as accommodation space for sediment increases, and may exceed the timescale of this study. From the perspective of the BIT index which monitors the relative input of terrestrial and marine organic matter, the exact source of the soil bacteria from within the basin delivered to the estuary is less important than for other proxies; although branched GDGT concentrations do vary amongst soils, and therefore possibly across the PR catchment, the BIT terrestrial end-member ratio is almost always > 0.9 (Hopmans et al., 2004 and subsequent references). Consequently, the time lag does not impact the BIT record significantly and, in terms of GDGT delivered to the estuary, episodic responses by individual tributaries to localised rainfall events are integrated over the entire basin. By contrast, not only can terrestrial concentrations of n-alcohols, n-fatty acids and sterols vary but also the end-member ratios, reflecting their derivation from compounds that have a much wider range of terrestrial and marine aquatic sources; thus, these parameters likely differ more dramatically across the

catchment. The terrestrial component of these records and $\delta^{13}C_{org}$ are therefore more vulnerable to changes in the source of the organic matter supplied and the associated transport time lag from source to estuary.

4.1 BIT index

The decrease in the BIT index from 6.5 ka to present could be interpreted either as recording an increase in marine thaumarchaeotal productivity or a decrease in the relative quantity of terrestrially-sourced organic matter to the Pearl River Estuary. Although an increase in marine productivity cannot be excluded without individual GDGT accumulation rates, the lack of any long-term increase in other putative marine (algal) biomarker concentrations (e.g. brassicasterol) makes this explanation of the data pattern unlikely.

In the modern Pearl River Estuary, surface sediment BIT indices exhibit a strong association with the sedimentary regime (Strong et al., 2012). Values are generally high across the delta front, ranging from 0.65 to 0.99, but decrease dramatically across the delta front - pro-delta transition (0.79-0.30, Fig. 1b) probably reflecting the lower, distal sedimentation rates (Fyfe et al., 1997; Zong et al., 2009). The core is located on the pro-delta area (Fig. 1b) and BIT values at the top of the core correspond well with those measured on modern samples closest to the core site (Figs. 1b & 3a). The BIT index at 6.5 ka is much higher (0.73-0.75) and similar to values observed in the Pearl River Estuary today at least 20 km up river from the core site (Fig. 1b).

There are two possible explanations for a decrease in terrestrially sourced organic matter over the past 6.5 ka: either it reflects significant (~20 km) erosion-driven regression of the deltaic system over the last 6.5 ka so that the location of the core became progressively more distal with time; or there has been a reduction in fluvial sediment flux delivered to the Pearl River Estuary. Sedimentary data from the Pearl River Estuary show that the delta has not undergone regression recently, but has instead prograded throughout the Holocene (Zong et al., 2009). However, Zong et al.'s (2009) study documents a gradual decline in delta progradation rate between 6.8-2 kyrs. This evolutionary history of the delta suggests that up until 2 ka, the decline in the BIT index reflects a reduction in the delivery of terrestrial organic matter (and other sediment) causing the rate of delta progradation to slow. This interpretation is also consistent both with the core's declining sedimentation rate (Yu et al.,

2012; Zong et al., 2010) and with the decline in the % clay through the core, which is fluvially derived and mirrors the BIT record (Fig. 6; Owen, 2005; Zong et al., 2009; Zong et al., 2006). A similar phenomenon has been observed in the Yangtze River Delta (Hori et al., 2001). During the last 2 kyrs, Zong et al (2009) describe a further decline in fluvial sediment delivery to the estuary as a consequence of on-going weakening of monsoonal discharge combined with human reclamation activity on the delta plain.

4.2 n-alcohol, n-fatty acid and sterol-based ratios

The large variations in the down-core records of *n*-alcohol (0.57-0.86; Fig. 3b), fatty acid (0.47-0.79) and sterol-based ratios (0.81-0.99) fall within the ranges that occur in the modern depositional environments in the Pearl River Estuary e.g. the delta plain, delta front and pro-delta regions (Strong et al., 2012). Modern sediments from the delta plain are dominated by high *n*-fatty acid, *n*-alcohol and sterol-based ratios, whereas pro-delta areas commonly have lower values for each of these ratios (Strong et al., 2012), and consequently these ratios might be expected to exhibit similar temporal trends as BIT indices and clay contents. Indeed, all four ratios exhibit an overall decrease with time. However, the *n*-fatty acid, *n*-alcohol and sterol-based ratios are also characterised by two additional features: a transient decrease in ratios around 5.5 ka and an interval of elevated but variable ratios from 3-2 ka. We therefore suggest that only some of their temporal trends can be explained by a simple model of reduced delta progradation that apparently accounts for the more systematic decline seen in the BIT index and clay record. Importantly, the *n*-fatty acid, *n*-alcohol and sterol-based ratios also track the down-core record of total organic carbon (%TOC; Fig. SI-6), suggesting that it is these particular terrigenous inputs that drive the total organic mass input to the PRE.

The BIT index is dependent on compounds deriving from a relatively narrow range of sources: putative soil bacteria and marine archaea. In comparison, the *n*-alcohol-, *n*-fatty acid- and sterol-based ratios derive from compounds that have a much wider range of terrestrial and marine aquatic sources and as a result reflect a more complex history than BIT. In particular, the putative marine components in the denominator of all three ratios (e.g. LMW *n*-alcohols or *n*-alkanoic acids) could have a range of sources, some of which are marine, but which could also include higher plants or soil bacteria. Consequently, changes in the relative terrigenous contributions to these inferred marine biomarkers resulting from localised rainfall and associated erosion in different parts of the Pearl River's large catchment would impact on the temporal trends shown in Figure 3. However, the parallel down-core

profiles of the *n*-alcohol-, *n*-fatty acid- and sterol-based ratios (Fig. 3b), suggest that these three ratios record the variation of a common source of organic matter. Given the wide and distinct range of potential sources of organic matter that could influence each of the ratios, the parallelism probably reflects the homogenising effect of sediment storage within a large, transport-limited catchment. Moreover, their similarity to the %TOC trends suggests that these ratios are not merely artefacts of unexpected end-member variations, but rather reflect a fundamental aspect of terrigenous organic matter delivery to the Pearl River estuary, albeit one that is partially decoupled from soil and sediment inputs.

We note that although these ratios represent compounds derived from a range of sources, the numerators are all primarily representative of higher plants, in contrast to the soil bacterial biomarker term in the BIT numerator. As such the differences between these ratios and the BIT index could arise from a different response of plant OM transport compared to soil OM. This could arise from subtle taxonomic shifts in vegetation type, which can change the leaf waxes and associated ratios significantly (Eglinton and Hamilton, 1967; Herbin and Robins, 1969; Holloway and Baker, 1970; Lytle et al., 1976). However, the plant biomarkers represented by the three ratios are rather physiologically diverse. In the *n*-alcohol and *n*-fatty acid-based ratios, the terrestrial component mainly derives from plant leaf waxes, and in the sterol-based ratio, the terrestrial component derives from a range of plant organic matter. As such, the fact that they exhibit similar trends suggests that the deviations from the BIT records predominantly reflect a decoupling between the quantity of soil OM relative to vegetation OM, rather than simply a change in species assemblage.

The mechanism for a decoupling of soil and land plant OM fluxes could be caused by changes in the amount of plant biomass, due to either climatic or agricultural impacts or a mechanistic decoupling of how the precipitation regime affects delivery of different types of OM to the fluvial system. For example, both sediment and plant matter will undergo enhanced erosion during high precipitation intensity events, but that might be especially true for the plant matter (Hilton et al., 2012), making its transport more susceptible to changes in seasonality. A related explanation could be different transport times of soil versus plant OM. As discussed earlier, sediment transport is likely to involve a significant residence time within the basin, and this could lead to an averaging out of short-term changes in sediment discharge. Higher plant organic matter may also experience extended residence times in soils (Drenzek et al., 2007; Galy and Eglinton, 2011; Smittenberg et al., 2006), but it is possible

that this is less pronounced than for compounds actually produced in the soil and consequently, episodic discharge events are better captured by vegetation-based parameters. If this is correct, then the interval from 3 to 2 kyr reflects a time of relatively low but seasonally intense precipitation, a hypothesis to be explored in future work.

4.3 Comparison with bulk organic matter $\delta^{13}C$ values

A comparison between the *n*-alcohol ratios and the bulk organic $\delta^{13}C$ record from the same core (Yu et al., 2012; Yu, 2009) shows good coincidence between 6.5 ka - 2.0 ka (Fig. 5a). The parallel profiles shown in Figure 3b suggest that this covariance extends to the fatty acid- and sterol-based ratios and this is likely to result from a common control, probably changes in the relative terrestrial organic matter input. Between 2 ka and present there is a marked discrepancy between the bulk sediment $\delta^{13}C$ record which shows a shift to more enriched $\delta^{13}C$ values at ~2.0 ka (Fig. 5a) and the biomarker based records, all of which show relatively stable values over this period (Fig. 3b and 5a). The rapid transition to more ^{13}C-enriched sedimentary OM ~2.0 ka may result either from a change in the OM flux or in the isotopic composition of the terrestrial and/or marine end member, such as a change in the former driven by a shift in C_3 and C_4 plant contributions (Yu et al., 2012). Compound specific $\delta^{13}C$ values allow us to test that hypothesis.

The generally low (-28 to -35 ‰) $\delta^{13}C$ values of high molecular weight (HMW) *n*-fatty acids (Fig. 5b) are consistent with an origin from C_3 plant leaf waxes (-28 to -37 ‰; Collister et al., 1994; Lockheart et al., 1997), rather than C_4 and CAM (Crassulacean acid metabolism) plant leaf waxes (-4 to -22 ‰; Bianchi and Bianchi, 1990; Chikaraishi and Naraoka, 2003; Chikaraishi and Naraoka, 2007; Collister et al., 1994; Conte et al., 2003). This dominance of C_3 plants is consistent with the known modern and Quaternary vegetation in the Pearl River basin (Winkler and Wang, 1993), in which C_3 forests dominate and C_4 plants such as grasses and agricultural sugar cane are minor contributors.

The rapid increase in bulk sediment $\delta^{13}C$ values at 2 ka (Yu et al., 2012) is mirrored by a similar shift in the $\delta^{13}C$ values of high molecular weight (HMW) *n*-fatty acids (Fig. 5b). The increase coincides with a plant lipid biomarker $\delta^{13}C$ record from a peat bog in northern China (Yamamoto et al., 2010), which records a rapid 2-3‰ enrichment in HMW *n*-alkanes at approximately 2 ka. Because the biomarker records derive solely from terrigenous (i.e. leaf wax) inputs, it confirms that the bulk organic matter isotopic shift arises from a change in the

terrigenous end member rather than a change in marine versus terrestrial mixing ratios. Such a change in higher plant biomarker $\delta^{13}C$ values can arise from changes in the vegetation composition, climatic impacts on isotope discrimination during photosynthesis or a combination of the two. For instance, ~2‰ variability in the $\delta^{13}C$ values of C_3 plant leaf waxes has previously been attributed to changes in mean annual precipitation, although temperature and altitude also impose controls (Arens et al., 2000; Diefendorf et al., 2010; Freeman et al., 2011; Miller et al., 2001; Warren et al., 2001). If moisture availability decreased at 2.0 ka, this could have led to ^{13}C-enrichment of C_3 plants, including their leaf waxes (Diefendorf et al., 2010; Freeman et al., 2011; Kohn, 2010; Van de Water et al., 2002). However, such impacts are generally less than 3-4‰ (e.g. Diefendorf et al., 2010), and although we do not preclude such changes in the isotopic composition of the C_3 plant community in the Pearl River basin, such a mechanism would require a dramatic change in the ecosystem and climate regime in order to fully explain the 3-4‰ enrichment recorded by the leaf waxes in this study (Fig. 5b).

C_4 plants are better adapted to warmer, drier conditions than C_3 plants. As a result C_4 plants generally increase in relative abundance as precipitation in a region decreases (Kristen et al., 2010; Pyankov et al., 2010; Wang, 2002), and this has been recorded in regions influenced by the Asian monsoon (Liu and Huang, 2005). Due to their high $\delta^{13}C$ values relative to those of C_3 plants, an increase in C_4 plants can also significantly (up to 6‰) enrich the bulk and leaf wax $\delta^{13}C$ signature of soils and sediments (Ding and Yang, 2000; Lichtfouse et al., 1994; Liu and Huang, 2005; Mo et al., 2004). The enrichment measured at 2.0 ka could therefore be a moisture-driven change in C_3 and C_4 plant contributions. A change in sediment source reflecting the enhanced erosion of drier areas of the basin, could result in a similar change in the carbon isotopic composition of Pearl River Estuary organic matter. However, since the Pearl River drainage basin currently has very low abundances of naturally-occurring C_4 plants (Winkler and Wang, 1993), it is unlikely that natural vegetation assemblage changes drove the observed $\delta^{13}C$ records by either of these mechanisms.

Instead, we suggest that the rapid enrichment of higher plant organic matter at 2.0 ka is anthropogenic (Zong et al., 2010). Agricultural practices in Southern China increased significantly from approximately 2.5-2.3 ka to present (Chi and Hung, 2010; Zong and al, in press) . Sugar cane, maize and other C_4 plants, with bulk $\delta^{13}C$ values of -10.6 to -16.1‰, (Yu et al., 2012; Yu, 2009; Zong and al, in press; Zong et al., 2010 and references therein) and

leaf wax $\delta^{13}C$ values of -4 to -22 ‰ (Bianchi and Bianchi, 1990; Chikaraishi and Naraoka, 2003; Chikaraishi and Naraoka, 2007; Collister et al., 1994; Conte et al., 2003), are native to the Pearl River basin, but are now abundant as a result of being some of the main cultivated crops in the lowlands of the basin. Yu (2009) and Zong et al (2010) suggested that anthropogenic enhancement of C_4 plants was a possible cause of the enrichment in the Pearl River Estuary bulk $\delta^{13}C$ values at 2.0 ka. Such an interpretation is also consistent with Holocene vegetation change inferred from China, including a significant reduction in deciduous C_3 tree pollen coinciding with an increase in charcoal from 2.0 ka to present, suggesting significant deforestation and biomass burning that could be associated with increased agriculture (Zhao et al., 2010). The same interpretation has been invoked for a speleothem-derived $\delta^{13}C_{org}$ record from the Xianshui Cave within the Pearl River catchment (Fig. 1) that exhibits a ~5‰ enrichment initiating at approximately 1.5 ka (Zhang et al., 2004). It seems likely therefore that climate is not the fundamental control on these records but rather, they provide further evidence of the widespread impact of developing agriculture.

4.4 Comparison with Dongge and other records

Speleothem oxygen isotope records are a function of both of the $\delta^{18}O$ of the precipitation and fractionation during evaporation (Fang, 1991; Huang et al., 1997). Consequently, instead of responding to declining precipitation, the Dongge record could reflect either a component of late Holocene cooling, or a different rainfall source (Maher and Tompson, 2012). Since the Pearl River Estuary records of bulk sediment carbon isotopes and the *n*-alcohol, *n*-fatty acid- and sterol-based ratios do not respond either to temperature or to rainfall source, it is possible that the differences between these records and Dongge.

However, consideration of the Pearl River and Dongge Cave records together has two important implications. First, the parallelism of the two records (Fig. 3a) suggests that despite differences in basin size, both records are dominated by common drivers. Second, if the BIT-derived MBT-CBT mean annual air temperatures throughout the core are representative of ~coeval branched GDGT synthesis over the last 6 kyrs, these are within error of modern temperatures. Moreover, although there is a large calibration error in MBT-CBT-derived MATs, the relative error for a single region is likely to be much lower (e.g. Peterse et al., 2012), such that the lack of any significant down-core change (the average for all data is 15.3 ºC with a 0.4 ºC standard deviation) is compelling evidence that there has been no significant cooling since 6.5 ka. Collectively, these data suggest that the Dongge

record does not reflect cooling and if there is a change in the rainfall source (Maher and Tompson, 2012), this is also mirrored by a decline in rainfall intensity. The inference we can draw from the similarity of the Dongge speleothem and Pearl River Estuary BIT records is therefore that they document a significant decrease in moisture transport from the mid-Holocene to 2 ka affecting a large part of South East Asia.

Considering the Dongge and BIT records together also helps determine whether the BIT indices record an overall precipitation change or basin-scale changes in the episodic and/or seasonal aspects of precipitation intensity (cf. Kelly et al., 2006), as both these strongly affect the relationship between water discharge and sediment load (Brennan and Wilson, 1993; Sfriso et al., 1992; Zhang et al., 2008). Since storage and mixing in the vadose zone dampens seasonal and shorter periodicity variations in the speleothem-recorded $\delta^{18}O$ signal of soil water (Ayalon et al., 1998; Yonge et al., 1985), the similarity of the Dongge $\delta^{18}O$ and BIT records suggests that the BIT record is not responding to changes in the seasonal pattern of rainfall intensity, but rather to a decline in overall precipitation and associated runoff..

We conclude therefore that both the BIT record from the Pearl River Estuary and the Dongge cave $\delta^{18}O$ speleothem records are recording regional palaeoprecipitation changes over the last 6.5 ka. This contrasts with the Pearl River Estuary $\delta^{13}C$ bulk organic carbon record which reflects a combined signal of regional declining palaeoprecipitation and changing organic matter content. From the perspective of model-data comparison, the BIT and Dongge cave records are therefore the most appropriate to use.

4.5 Model-data comparison

Climate simulations generated as part of the Palaeoclimate Model Intercomparison Project (PMIP2; Braconnot et al., 2003; Crucifix et al., 2005; Harrison et al., 2002) used coupled ocean-atmosphere General Circulation Models to investigate the mid-Holocene. Tao et al (2010) showed that all twelve PMIP2 models predicted warmer conditions in East Asia for the mid-Holocene than preindustrial. However, analysis of model results for the region between 95E and 115E, and 22N to 28N (a rectangular region approximating the Pearl River drainage basin represented by up to 15 model grid squares) shows that despite the relative warmth of the mid-Holocene regionally, this area is characterised by minimal change in surface air temperature (~1^{o}C), particularly in the summer months (JJAS; Fig. 7a). Tao et al

(2010) undertook a model-data comparison exercise to test their East Asian model results, but they had no data from the Pearl River basin. We can now confirm that this localised area of relatively cool mid-Holocene temperatures, which may result from an enhanced hydrological cycle in the area, is consistent with the MBT-CBT-derived mean annual air temperatures from the Pearl River estuary core.

Wind anomalies derived from PMIP2 simulations of the mid-Holocene are indicative of a strong summer monsoon (Tao et al., 2010) with increased water vapour transport, particularly in South China (Zhao et al., 2007). Inter-model comparison of the East Asian precipitation responses of the different PMIP2 models to the same mid-Holocene forcings shows considerable variation and some disagreement with the available proxy data (Tao et al., 2010). Variability is also seen in the modelled precipitation for the grid cells covering the Pearl River basin. However, of the 7 simulations for which there are data for both precipitation and runoff, all yield wetter JJAS results for the mid-Holocene (Fig. 7b) and associated elevated runoff (Fig. 7c). The same pattern is seen in the annual mean precipitation with the exception of the FOAM and, to a lesser extent, the MRI-CGCM2.3.4nfa models (Fig. 7; Tao et al., 2010). The basin-scale of the BIT data permits spatially-equivalent model-data comparison for the first time. This comparison indicates that the majority of model simulations show a decline in precipitation and associated runoff with time and are consistent with our interpretation of the Dongge and BIT records. This allows us to discriminate between models and suggest that the FOAM and MRI-CGCM2.3.4nfa models are not capturing the hydrological cycle in this area well. An expansion of this approach to include BIT records for the other major river basins along the East Asian margin will permit mapping of the Summer Asian Monsoon intensity with time and should help discriminate robustly between model simulations.

5 Conclusions

The biomarker and compound-specific $\delta^{13}C$ records generated on a core from the Pearl River Estuary, SE China, provide new insights into the behaviour of the Pearl River over the last six and half thousand years. The integration of these new datasets with published records resolves some of the outstanding problems associated with the interpretation of existing data. These include:

1. The GDGT-derived MBT-CBT mean annual air temperatures suggest negligible temperature change over the last 6.5 kyrs, supporting the interpretation of the Dongge speleothem $\delta^{18}O$ data as a record of changing precipitation (Tao et al., 2010).
2. There is a clear parallelism between the small-scale Dongge speleothem and the more regional Pearl River Estuary BIT record. Although sedimentological change in the Pearl River Estuary is governed by a range of climatic variables, modulated through potentially complex catchment dynamics, the overall similarity of the two records suggests they share a common precipitation-driven control derived from the regional climate signal.
3. Plant-based biomarker ratios indicate a more complex pattern of change in terrestrial organic matter delivery to the Pearl River Estuary. This suggests that branched GDGT transport is closely associated with sediments, which is consistent with its origin in soils, whereas vegetation transport can become partially decoupled from sediment transport, perhaps during intense episodic events. Importantly, this pool of vegetation-derived organic matter appears to drive the total organic matter burial in the Pearl River estuary.
4. Leaf wax $\delta^{13}C$ values indicate that the dominant vegetation in the Pearl River catchment has changed, with significant impacts on interpretation of $\delta^{13}C_{org}$ records after 2 ka. The change in basin vegetation around 2 ka probably resulted from anthroprogenic cultivation of maize and sugar cane in lowland areas. This could provide an additional control on drainage basin processes but also highlights the important relationship between monsoon intensity and the habitability of the Pearl River basin.
5. Scale-equivalent comparison of temperature, precipitation and runoff data is consistent with the majority of PMIP2 climate models' output from the grid cells representing the Pearl River basin.

Taken together, the records of sedimentological change in the Pearl River Basin, changes in Dongge Cave speleothem oxygen isotopes (and associated lack of evidence for temperature change), and decreased modelled runoff all suggest a decline in moisture transport from the mid-Holocene to 2 ka across SE Asia.

An, C.B., Feng, Z.D., Tang, L.Y., 2004. Environmental change and cultural response between 8000 and 4000 cal. yr BP in the western Loess Plateau, northwest China. Journal of Quaternary Science 19, 529-535.
Arens, N.C., Jahren, A.H., Amundson, R., 2000. Can C3 plants faithfully record the carbon isotopic composition of atmospheric carbon dioxide? Paleobiology 26, 137-164.

Ayalon, A., Bar-Matthews, M., Sass, E., 1998. Rainfall-recharge relationships within a karstic terrain in the eastern Mediterranean semi-arid region, Israel: delta O-18 and delta D characteristics. Journal of Hydrology 207, 18-31.
Bendle, J.A., Weijers, J.W.H., Maslin, M.A., Damste, J.S.S., Schouten, S., Hopmans, E.C., Boot, C.S., Pancost, R.D., 2010. Major changes in glacial and Holocene terrestrial temperatures and sources of organic carbon recorded in the Amazon fan by tetraether lipids. Geochemistry Geophysics Geosystems 11.
Bianchi, A., Bianchi, G., 1990. Surface lipid composition of C-3 and C-4 plants Biochemical Systematics and Ecology 18, 533-537.
Bourbonniere, R.A., Meyers, P.A., 1996. Sedimentary geolipid records of historical changes in the watersheds and productivities of Lakes Ontario and Erie. Limnology and Oceanography 41, 352-359.
Braconnot, P., Joussaume, S., Harrison, S., Hewitt, C., Valdes, P.J., Ramstein, G., Stouffer, R.J., Otto-Bliesner, B., Taylor, K.E., 2003. The second phase of the Paleoclimate Modeling Intercomparison Project (PMIP II). Clivar Exchanges 8, 19-20.
Brennan, B.M., Wilson, J.G., 1993. Spatial and temporal variation in sediments and their nutrient concentrations in the unpolluted Shannon estuary, Ireland. Archiv fuer Hydrobiologie Supplementband 75, 451-486.
Cai, W.J., M., D., Wang, Y., Zhai, W., Huang, T., Chen, S., Zhang, F., Chen, Z., Wang, Z.D., 2004. The biogeochemistry of inorganic carbon and nutrients in the Pearl River estuary and the adjacent northern South China Sea. Continental Shelf Research 24, 1301-1319.
Chi, Z., Hung, H.-c., 2010. The emergence of agriculture in southern China. Antiquity 84, 11-25.
Chikaraishi, Y., Naraoka, H., 2003. Compound-specific dD–d13C analyses of n-alkanes extracted from terrestrial and aquatic plants. Phytochemistry 63, 361-371.
Chikaraishi, Y., Naraoka, H., 2007. [delta]13C and [delta]D relationships among three n-alkyl compound classes (n-alkanoic acid, n-alkane and n-alkanol) of terrestrial higher plants. Organic Geochemistry 38, 198-215.
CMDSSS, 2011. (China Meteorological Data Sharing Service System), China Climate Normal Dataset (1971-2000) National Meteorological Information Center, China.
Collister, J.W., Rieley, G., Stern, B., Eglinton, G., Fry, B., 1994. Compound-Specific Delta-C-13 Analyses of Leaf Lipids from Plants with Differing Carbon-Dioxide Metabolisms. Organic Geochemistry 21, 619-627.
Conte, M.H., Weber, J.C., Carlson, P.J., Flanagan, L.B., 2003. Molecular and carbon isotopic composition of leaf wax in vegetation and aerosols in a northern prairie ecosystem. Oecologia 135, 67-77.
Crucifix, M., Braconnot, P., Harrison, S., Otto-Bliesner, B., 2005. Second phase of the Paleoclimate Modelling Intercomparison Project. EOS, Transactions of the American Geophysical Union 86.
Diefendorf, A.F., Mueller, K.E., Wing, S.L., Koch, P.L., Freeman, K.H., 2010. Global patterns in leaf C-13 discrimination and implications for studies of past and future climate. Proceedings of the National Academy of Sciences of the United States of America 107, 5738-5743.
Ding, Z.L., Yang, S.L., 2000. C-3/C-4 vegetation evolution over the last 7.0 Myr in the Chinese Loess Plateau: evidence from pedogenic carbonate delta C-13. Palaeogeography Palaeoclimatology Palaeoecology 160, 291-299.

Dong, J.G., Wang, Y.J., Cheng, H., Hardt, B., Edwards, R.L., Kong, X.G., Wu, J.Y., Chen, S.T., Liu, D.B., Jiang, X.Y., Zhao, K., 2010. A high-resolution stalagmite record of the Holocene East Asian monsoon from Mt Shennongjia, central China. Holocene 20, 257-264.
Drenzek, N.J., Montlucon, D.B., Yunker, M.B., Macdonald, R.W., Eglinton, T.I., 2007. Constraints on the origin of sedimentary organic carbon in the Beaufort Sea from coupled molecular C-13 and C-14 measurements. Marine Chemistry 103, 146-162.
Eglinton, G., Hamilton, R.J., 1967. Leaf Epicuticular Waxes. Science 156, 1322-&.
Fabbri, D., Sangiorgi, F., Vassura, I., 2005. Pyrolysis-GC-MS to trace terrigenous organic matter in marine sediments: a comparison between pyrolytic and lipid markers in the Adriatic Sea. Analytica Chimica Acta 530, 253-261.
Fang, J.Q., 1991. Lake evolution during the past 30,000 years in China, and its implications for environmental change. Quaternary Research 36, 37-60.
Fang, J.S., Barcelona, M.J., Abrajano, T., Nogi, Y., Kato, C., 2002. Isotopic composition of fatty acids of extremely piezophilic bacteria from the Mariana Trench at 11,000 m. Marine Chemistry 80, 1-9.
Freeman, K.H., Colarusso, L.A., 2001. Molecular and isotopic records of C-4 grassland expansion in the late Miocene. Geochimica Et Cosmochimica Acta 65, 1439-1454.
Freeman, K.H., Mueller, K.E., Diefendorf, A.F., Wing, S.L., Koch, P.L., 2011. Clarifying the influence of water availability and plant types on carbon isotope discrimination by C3 plants. Proceedings of the National Academy of Sciences of the United States of America 108, E59-E60.
Fyfe, J.A., Selby, I.C., Shaw, R., James, J.W.C., Evans, C.D.R., 1997. Quaternary sea-level change on the continental shelf of Hong Kong. Journal of the Geological Society 154, 1031-1038.
Gagosian, R.B., Peltzer, E.T., 1986. Atmospheric transport of continentally derived organic material to the central Pacific Ocean. Atmospheric Environment 20, 2074.
Galy, V., Eglinton, T., 2011. Protracted storage of biospheric carbon in the Ganges-Brahmaputra basin. Nature Geoscience 4, 843-847.
Gogou, A., Stephanou, E.G., 2004. Marine organic geochemistry of the Eastern Mediterranean: 2. Polar biomarkers in Cretan Sea surficial sediments. Marine Chemistry 85, 1-25.
Harrison, S., Braconnot, P., Hewitt, C., Stouffer, R.J., 2002. Fourth international workshop of the Paleoclimate Modelling Intercomparison Project (PMIP): launching PMIP Phase II. EOS 83, 447.
Hedges, J.I., Oades, J.M., 1997. Comparative organic geochemistries of soils and marine sediments. Organic Geochemistry 27, 319-361.
Herbin, G.A., Robins, P.A., 1969. Patterns of variation and development in leaf wax alkanes. Phytochemistry 8, 1985-&.
Hilton, R.G., Galy, A., Hovius, N., Kao, S.J., Horng, M.J., Chen, H., 2012. Climatic and geomorphic controls on the erosion of terrestrial biomass from subtropical mountain forest. Global Biogeochemical Cycles 26.
Holloway, P.J., Baker, E.A., 1970. Cuticles of some Angiosperm leaves and fruits. Annals of Applied Biology 66, 145-&.
Hopmans, E.C., Weijers, J.W.H., Schefuss, E., Herfort, L., Damste, J.S.S., Schouten, S., 2004. A novel proxy for terrestrial organic matter in sediments based on branched and isoprenoid tetraether lipids. Earth and Planetary Science Letters 224, 107-116.

Hori, K., Saito, Y., Zhao, Q., Cheng, X., Wang, P., Sato, Y., Li, C., 2001. Sedimentary facies and Holocene progradation rates of the
Changjiang (Yangtze) delta, China. Geomorphology 41, 233–248.
Hu, J.F., Peng, P.A., Chivas, A.R., 2009. Molecular biomarker evidence of origins and transport of organic matter in sediments of the Pearl River estuary and adjacent South China Sea. Applied Geochemistry 24, 1666-1676.
Huang, C.Y., Liew, P.M., Zhao, M.Q., Chang, T.C., Kuo, C.M., Chen, M.T., Wang, C.H., Zheng, L.F., 1997. Deep sea and lake records of the Southeast Asian paleomonsoons for the last 25 thousand years. Earth and Planetary Science Letters 146, 59-72.
Jones, J.G., 1969. Studies on Lipids of Soil Micro-Organisms with Particular Reference to Hydrocarbons. Journal of General Microbiology 59, 145.
Kelly, M.J., Edwards, R.L., Cheng, H., Yuan, D., Cai, Y., Zhang, M., 2006. High resolution characterization of the Asian Monsoon between 146,000 and 99,000 years B.P. from Dongge Cave, China and global correlation of events surrounding Termination II. Palaeogeography, Palaeoclimatology,
Palaeoecology 236, 20-38.
Kohn, M.J., 2010. Carbon isotope compositions of terrestrial C3 plants as indicators of (paleo)ecology and (paleo)climate. Proceedings of the National Academy of Sciences of the United States of America 107, 19691-19695.
Kristen, I., Wilkes, H., Vieth, A., Zink, K.G., Plessen, B., Thorpe, J., Partridge, T.C., Oberhansli, H., 2010. Biomarker and stable carbon isotope analyses of sedimentary organic matter from Lake Tswaing: evidence for deglacial wetness and early Holocene drought from South Africa. Journal of Paleolimnology 44, 143-160.
Li, P., Qiao, P., Zheng, H., Fang, G., Huang, G., 1991. The environmental evolution of the Pearl River Delta in the last 10,000 years. China Ocean Press (in Chinese).
Lichtfouse, E., Elbisser, B., Balesdent, J., Mariotti, A., Bardoux, G., 1994. Isotope and molecular evidence for direct input of maize leaf wax n-alkanes into crop soils. Organic Geochemistry 22, 349-351.
Liu, W., Huang, Y., 2005. Compound specific D/H ratios and molecular distributions of higher plant leaf waxes as novel paleoenvironmental indicators in the Chinese Loess Plateau. Organic Geochemistry 36, 851–860.
Lockheart, M.L., van Bergen, P.F., Evershed, R.P., 1997. Variations in the stable carbon isotope compositions of individual lipids from the leaves of modern angiosperms: implications for the study of higher land plant-derived sedimentary organic matter. Organic Geochemistry 26, 137-153.
Lunt, D.J., Flecker, R., Valdes, P.J., Salzmann, U., Gladstone, R., Haywood, A.M., 2008. A methodology for targeting palaeo proxy data acquisition: A case study for the terrestrial late Miocene. Earth and Planetary Science Letters 271, 53–62.
Lytle, T.F., Lytle, J.S., Caruso, A., 1976. Hydrocarbons and fatty-acids of ferns. Phytochemistry 15, 965-970.
Maher, B., Tompson, R., 2012. Oxygen isotopes from Chinese caves: records not of monsoon rainfall but of circulation regime. Journal of Quaternary Science 27, 615-624.
Markwick, P.J., Valdes, P.J., 2004. Palaeo-digital elevation models for use as boundary conditions in coupled ocean-atmosphere GCM experiments: a Maastrichtian (late Cretaceous) example. Palaeogeography, Palaeoclimatology, Palaeoecology 213, 37-63.

McCaffrey, M.A., Farrington, J.W., Repeta, D.J., 1991. The Organic Geochemistry of Peru Margin Surface Sediments .2. Paleoenvironmental Implications of Hydrocarbon and Alcohol Profiles. Geochimica Et Cosmochimica Acta 55, 483-498.
Miller, J.M., Williams, R.J., Farquhar, G.D., 2001. Carbon isotope discrimination by a sequence of Eucalyptus species along a subcontinental rainfall gradient in Australia. Functional Ecology 15, 222-232.
Mo, W., Nishimura, N., Soga, Y., Yamada, K., Yoneyama, T., 2004. Distribution of C3 and C4 plants and changes in plant and soil carbon isotope ratios with altitude in the Kirigamine grassland, Japan. Grassland Science 50, 243-254.
Nishimura, M., Baker, E.W., 1986. Possible Origin of N-Alkanes with a Remarkable Even-to-Odd Predominance in Recent Marine-Sediments. Geochimica Et Cosmochimica Acta 50, 299-305.
Owen, R.B., 2005. Modern fine-grained sedimentation - spatial variability and environmental controls on an inner pericontinental shelf. Marine Geology 214, 1-26.
Peterse, F., van der Meer, J., Schouten, S., Weijers, J.W.H., Fierer, N., Jackson, R.B., Kim, J.-H., Damste, J.S.S., 2012. Revised calibration of the MBT-CBT paleotemperature proxy based on branched tetraether membrane lipids in surface soils. Geochimica Et Cosmochimica Acta 96, 215-229.
Pyankov, V.I., Ziegler, H., Akhani, H., Deigele, C., Luttge, U., 2010. European plants with C-4 photosynthesis: geographical and taxonomic distribution and relations to climate parameters. Botanical Journal of the Linnean Society 163, 283-304.
Schouten, S., Hopmans, E.C., Pancost, R.D., Damste, J.S.S., 2000. Widespread occurrence of structurally diverse tetraether membrane lipids: Evidence for the ubiquitous presence of low-temperature relatives of hyperthermophiles. Proceedings of the National Academy of Sciences of the United States of America 97, 14421-14426.
Sfriso, A., Pavoni, B., Marcomini, A., Raccanelli, S., Orio, A.A., 1992. Particulate matter deposition and nutrient fluxes onto the sediments of the Venice Lagoon. Environmental Technology 13, 473-483.
Shi, Y.F., Kong, Z.Z., Wang, S.M., Tang, L.Y., Wang, F.B., Yao, T.D., Zhao, X.T., Zhang, P.Y., Shi, S.H., 1994. The climatic fluctuation and important events of holocene megathermal in China. Science in China Series B - Chemistry 37, 353-365.
Sinninghe-Damsté, J.S., Ossebaar, J., Schouten, S., Verschuren, D., 2008. Altitudinal shifts in the branched tetraether lipid distribution in soil from Mt. Kilimanjaro (Tanzania): Implications for the MBT/CBT continental palaeothermometer Organic Geochemistry 39, 1072-1076.
Smittenberg, R.H., Eglinton, T.I., Schouten, S., Damste, J.S.S., 2006. Ongoing buildup of refractory organic carbon in boreal soils during the Holocene. Science 314, 1283-1286.
Strong, D.J., Flecker, R.M., Valdes, P.J., Wilkinson, I.P., Rees, J.G., Zong, Y.Q., Lloyd, J.M., Garrett, E., Pancost, R.D., 2012. Organic matter distribution in the modern sediments of the Pearl River Estuary. Organic Geochemistry 49, 68-82.
Tao, W., Huijun, W., Dabang, J., 2010. Mid-Holocene East Asian summer climate as simulated by the PMIP2 models. Palaeogeography, Palaeoclimatology, Palaeoecology 288, 93-102.
Tierney, J.E., Russell, J.M., 2009. Distributions of branched GDGTs in a tropical lake system: Implications for lacustrine application of the MBT/CBT paleoproxy. Organic Geochemistry 40, 1032-1036.
Tierney, J.E., Russell, J.M., Eggermont, H., Hopmans, E.C., Verschuren, D., Damste, J.S.S., 2010. Environmental controls on branched tetraether lipid

distributions in tropical East African lake sediments. Geochimica Et Cosmochimica Acta 74, 4902-4918.
Van de Water, P.K., Leavitt, S.W., Betancourt, J.L., 2002. Leaf delta C-13 variability with elevation, slope aspect, and precipitation in the southwest United States. Oecologia 132, 332-343.
Volkman, J.K., 1986. A Review of Sterol Markers for Marine and Terrigenous Organic-Matter. Organic Geochemistry 9, 83-99.
Volkman, J.K., Barrett, S.M., Blackburn, S.I., 1999. Eustigmatophyte microalgae are potential sources of C-29 sterols, C-22-C-28 n-alcohols and C-28-C-32 n-alkyl diols in freshwater environments. Organic Geochemistry 30, 307-318.
Volkman, J.K., Barrett, S.M., Blackburn, S.I., Mansour, M.P., Sikes, E.L., Gelin, F., 1998. Microalgal biomarkers: A review of recent research developments. Organic Geochemistry 29, 1163-1179.
Wang, P.X., Clemens, S., Beaufort, L., Braconnot, P., Ganssen, G., Jian, Z.M., Kershaw, P., Sarnthein, M., 2005. Evolution and variability of the Asian monsoon system: state of the art and outstanding issues. Quaternary Science Reviews 24, 595-629.
Wang, R.Z., 2002. Photosynthetic pathways and life forms in different grassland types from North China. Photosynthetica 40, 243-250.
Warren, C.R., McGrath, J.F., Adams, M.A., 2001. Water availability and carbon isotope discrimination in conifers. Oecologia 127, 476-486.
Webster, P.J., Magana, V.O., Palmer, T.N., Shukla, J., Tomas, R.A., Yanai, M., Yasunari, T., 1998. Monsoons: Processes, predictability, and the prospects for prediction. Journal of Geophysical Research - Oceans 103, 14451-14510.
Weijers, J.W.H., Schouten, S., Schefuss, E., Schneider, R.R., Damste, J.S.S., 2009. Disentangling marine, soil and plant organic carbon contributions to continental margin sediments: A multi-proxy approach in a 20,000 year sediment record from the Congo deep-sea fan. Geochimica Et Cosmochimica Acta 73, 119-132.
Weijers, J.W.H., Schouten, S., van den Donker, J.C., Hopmans, E.C., Damste, J.S.S., 2007. Environmental controls on bacterial tetraether membrane lipid distribution in soils. Geochimica Et Cosmochimica Acta 71, 703-713.
Winkler, M.G., Wang, P.K., 1993. The late-Quaternary vegetation and climate of China. Global climates since the last glacial maximum, 221-264.
Yamamoto, S., Kawamura, K., Seki, O., Meyers, P.A., Zheng, Y., Zhou, W., 2010. Paleoenvironmental significance of compound-specific [delta]13C variations in n-alkanes in the Hongyuan peat sequence from southwest China over the last 13 ka. Organic Geochemistry 41, 491-497.
Yancheva, G., Nowaczyk, N.R., Mingram, J., Dulski, P., Schettler, G., Negendank, J.F.W., Liu, J.Q., Sigman, D.M., Peterson, L.C., Haug, G.H., 2007. Influence of the intertropical convergence zone on the East Asian monsoon. Nature 445, 74-77.
Yonge, C.J., Ford, D.C., Gray, J., Schwarcz, H.P., 1985. Stable isotope studies of cave seepage water. Chemical Geology 58, 97-105.
Yu, F., Zong, Y., Lloyd, J.M., Leng, M., Switzer, A.D., Yim, W.W.S., Huang, G., 2012. Mid-Holocene variability of the East Asian monsoon based on bulk organic δ13C and C/N records from the Pearl River estuary, southern China. Holocene 22, 705-715.
Yu, F.L., 2009. Reconstruction of the East Asian monsoon variability since the mid-Holocene from the Pearl River estuary, southern China, Geography. Durham University, Durham.

Zhang, M.L., Yuan, D.X., Lin, Y.S., Qin, J.M., Bin, L., Cheng, H., Edwards, R.L., 2004. A 6000-year high-resolution climatic record from a stalagmite in Xiangshui Cave, Guilin, China. Holocene 14, 697-702.
Zhang, S.R., Lu, X.X., Higgitt, D.L., Chen, C.T.A., Han, J.T., Sun, H.G., 2008. Recent changes of water discharge and sediment load in the Zhujiang (Pearl River) Basin, China. Global and Planetary Change 60, 365-380.
Zhao, P., Zhu, Y., Zhang, R., 2007. An Asian-Pacific teleconnection in summer tropospheric temperature and associated Asian climate variability. Climate Dynamics 28, 533-551.
Zhao, Y., Chen, F.H., Zhou, A.F., Yu, Z.C., Zhang, K., 2010. Vegetation history, climate change and human activities over the last 6200 years on the Liupan Mountains in the southwestern Loess Plateau in central China. Palaeogeography Palaeoclimatology Palaeoecology 293, 197-205.
Zong, Y., 2004. Mid-Holocene sea-level highstand along the Southeast Coast of China. Quaternary International 117, 55-67.
Zong, Y., al, e., in press. Changes in sea level, water salinity and wetland habitat linked to the late agricultural development in the Pearl River delta plain of China. Quaternary Science Reviews.
Zong, Y., Huang, G., Switzer, A.D., Yu, F., Yim, W.W.S., 2009. An evolutionary model for the Holocene formation of the Pearl River delta, China. Holocene 19, 129-142.
Zong, Y., Lloyd, J.M., Leng, M.J., Yim, W.W.S., Huang, G., 2006. Reconstruction of Holocene monsoon history from the Pearl River Estuary, southern China, using diatoms and carbon isotope ratios. Holocene 16, 251-263.
Zong, Y., Yu, F., Huang, G., Lloyd, J.M., Yim, W.W.S., 2010. Sedimentary evidence of Late Holocene human activity in the Pearl River delta, China. Earth Surface Processes and Landforms 35, 1095-1102.

Figure captions for Strong et al QSR

Fig. 1 – (a) Pearl River drainage basin with sites of previously published paleoprecipitation proxy records (back circles) from lakes (Toushe, Huang et al. 1997), caves (Dongge, Wang et al. 2005; Sanbao, Dong et al. 2010; Xiangshui, Zhang et al. 2004, and Panlong, Li Bin et al., 1996) and pollen (Xifeng, Liu and Huang 2005; Sujiawan and Dadiwan, An et al. 2004). Black circles are larger than the catchment associated with the corresponding paleoprecipitation proxy record. 1.25°x1.25° box indicates the size of the cell size for a climate general circulation model such as HadCM3. (b) Pearl River Estuary showing modern BIT indices (circles) and the rapid transition across the delta toe (dashed line; after Strong et al., 2012). The location of the HKUV-1 core (©) is also shown. Its shading corresponds to BIT indices for the core surface (left) and 6.5 ka (right). The core was obtained through the Civil Engineering Department, Hong Kong SAR Government, China.

Fig. 2 – Comparison between Dongge Cave speleothem $\delta^{18}O$ (Wang et al., 2005), and Pearl River Estuary core bulk organic $\delta^{13}C$ (Yu et al., 2011), from 6.5ka-present. Arrows on the y-axis indicate the direction of increasing and decreasing precipitation (ppt).

Fig. 3 – (a) variation in the HKUV-1 sediment core BIT indices and Dongge Cave speleothem $\delta^{18}O$ (Wang et al., 2005). Error bars, derived from a reversal in the age model (see supplementary information) where different linear regressions can be taken through the dated points, are shown on some data points. Boxed BIT indices reflect four samples encompassing a brief period of apparent discrepancy between the two records; (b) records of sterol, *n*-alcohol and *n*-fatty acid ratios for the HKUV-1 core. Modern ranges taken from Strong et al (2012). The r^2 values for fatty acid vs *n*-alcohol ratios, sterol vs *n*-alcohol ratios and fatty acid vs sterol ratios are 0.88, 0.83 and 0.77 respectively.

Fig. 4 – Reconstruction of mean annual temperature (MAT) from MBT-CBT indices using the calibration of Peterse et al (2012). The calibration error for these temperatures is ± 4-5°C (Weijers et al., 2007a). The shaded area of the graph illustrates the range of MATs derived from analysis of modern samples across the Pearl River Estuary (Strong et al 2012) recalibrated using Peterse et al (2012).

Fig. 5 – Mid-Holocene to present record of (a) the *n*-alcohol ratio and bulk organic $\delta^{13}C$ values; (b) bulk organic $\delta^{13}C$ values (Yu et al., 2011) in comparison to compound-specific $\delta^{13}C$ values of $C_{26\text{-}34}$ *n*-fatty acids.

Fig. 6 - Comparison between the BIT index and %clay. The storm event at 1.2 ka has been removed from both records.

Fig. 7 – PMIP2 coupled atmosphere-ocean model simulation results for grid squares representing the Pearl River drainage basin: a) annual mean, winter (DJF) and summer (JJAS) surface air temperature for both mid Holocene (6k) and Preindustrial (PI) simulations; b) difference between the mid-Holocene and preindustrial precipitation; c) difference between mid Holocene and preindustrial runoff.

Supplementary information table captions

Table SI-1. GDGTs and compound-specific $\delta^{13}C$ values of $C_{26\text{-}34}$ *n*-fatty acids from Pearl River Estuary HKUV-1 core samples. The calibration equation used to calculate the mean annual temperature (MAT) is from Peterse et al (2012).

Table SI-2. Concentrations (in µg g-1) of n-alcohols extracted from Pearl River Estuary HKUV-1 core samples.

Table SI-3. Concentrations and concentration ratios of biomarkers found in Pearl Estuary HKUV-1 core samples.

Table SI-4. Concentrations (in µg g-1) of steroids extracted from Pearl River Estuary HKUV-1 core samples.

Table SI-5 Concentrations (in µg g-1) of n-fatty acids extracted from Pearl River Estuary HKUV-1 core samples.

Supplementary information figure captions

Fig. SI-1 Age model encompassing calibrated foraminiferal carbonate ^{14}C-derived dates (black dots) from Zong et al. (2009) and Yu (2009), and lines of regression (black lines) used to estimate sample ages; (a) regressions with all 7 dated points included with reversal indicated;(b) regressions with one of the reversal points (1.92 m) removed; (c) regressions with the other reversal point (2.61 m) removed.

Fig. SI-2 - Typical gas chromatograms from (a) a saturated fraction (sample UV997; 6.5 ka); (b) a neutral polar fraction (sample UV997; 6.5 ka); (c) an acid fraction from the lower core (sample UV997; 6.5 ka) and (d) an acid fraction from the upper core (UV063; 0.3 ka). Peaks marked with closed circles are a homologous series of *n*-alkanes in the saturated fraction, *n*-alcohols in the polar fraction and *n*-fatty acids in the acid fractions. Peaks marked with open circles are hopanoid compounds in the saturated fraction and steroid compounds in the neutral polar fraction. Peaks marked with an asterisk (*) are fatty acid methyl esters (FAMEs) in the polar fraction and diacids in the acid fractions. Peaks marked with (+) are diplopterol and C_{32} *bis*-homohopanol in the polar fraction and C_{32} *bis*-homohopanoic acid in the acid fraction.

Fig. SI-3 - HKUV-1 records from 6.5 ka to present of (a) high molecular weight (HMW, $C_{26\text{-}34}$) *n*-fatty acid Carbon Preference Index (CPI); (b) HMW *n*-alcohol CPI; (c) HMW *n*-fatty acid average chain length (ACL) and (d) HMW *n*-alcohol ACL.

Fig. SI-4 - HKUV-1 neutral polar fraction (a) high molecular weight (HMW, $C_{26\text{-}34}$) *n*-alcohol concentrations; (b) low molecular weight (LMW, C_{16+18}) *n*-alcohol concentrations; (c) the sum of C_{29} sterol and stanol concentrations; (d) brassicasterol concentrations; (e) high molecular weight (HMW, $C_{26\text{-}34}$) *n*-fatty acid concentrations; (f) low molecular weight (LMW, C_{16+18}) *n*-fatty acid concentrations.

Fig. SI-5 – Mid-Holocene to present record of (a) $\delta^{13}C$ values of C_{26}, C_{28} and C_{30} n-fatty acids;

Fig. SI-6 - Comparison between the n-alcohol ratio and %total organic carbon. The storm event at 1.2 ka is removed from all records.

References

Li Bin, Yuan Daoxian, Qin Jiaming, Meiliang, Z., Yushi, L., 1996. High resolution record of climate change in a stalagmite from Panlong Cave of Guilin since 36,000 years B.P., In: Lauriteeu, S.E. (Ed.), Climate change: the Karst Record. Karst Waters Institute Special Publications, Charles Town, WV, pp. 93-96.
Peterse, F., van der Meer, J., Schouten, S., Weijers, J.W.H., Fierer, N., Jackson, R.B., Kim, J.-H., Damste, J.S.S., 2012. Revised calibration of the MBT-CBT paleotemperature proxy based on branched tetraether membrane lipids in surface soils. Geochimica Et Cosmochimica Acta 96, 215-229.

Figure 1

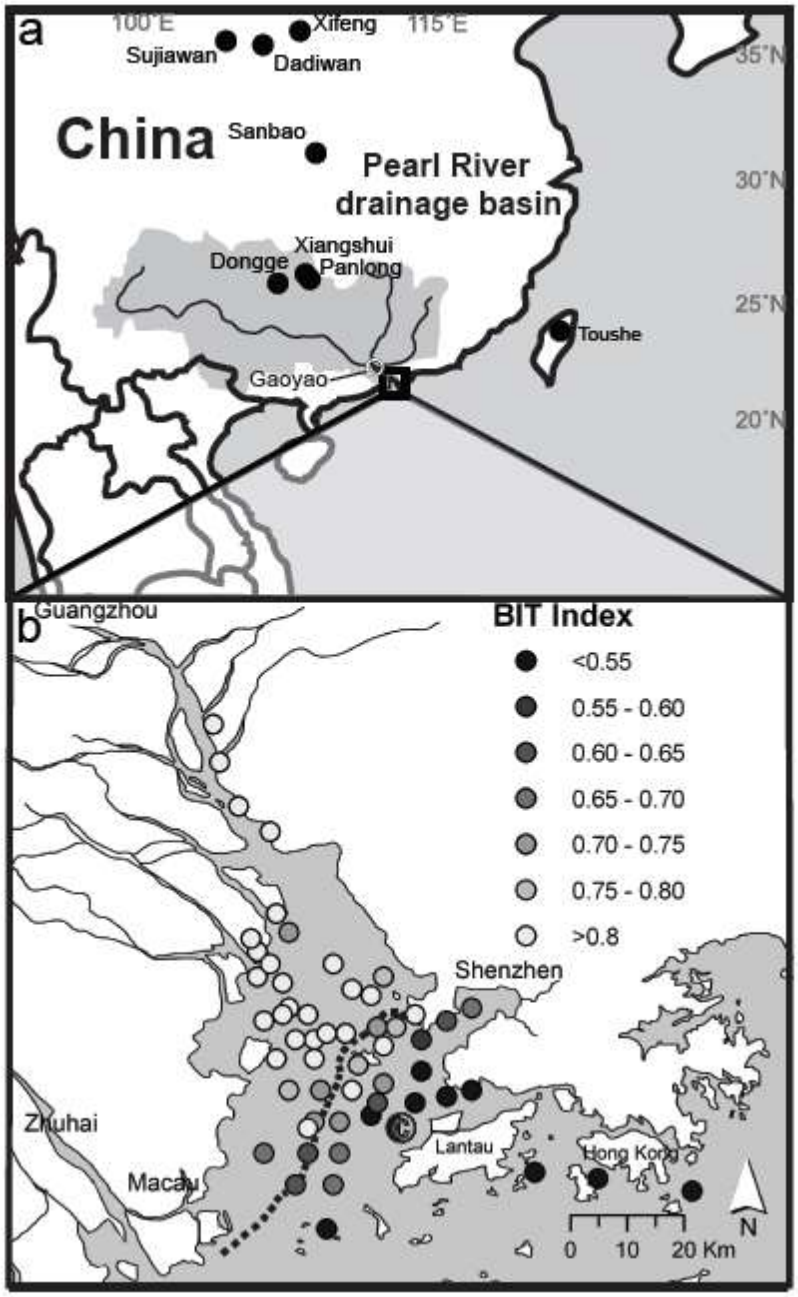
a
100°E
115°E
35°N
30°N
25°N
20°N
Xifeng
Sujiawan
Dadiwan
China
Sanbao
Pearl River
drainage basin
Xiangshui
Dongge
Panlong
Toushe
Gaoyao
b
Guangzhou
BIT Index
<0.55
0.55 - 0.60
0.60 - 0.65
0.65 - 0.70
0.70 - 0.75
0.75 - 0.80
>0.8
Shenzhen
Zhuhai
Lantau
Hong Kong
Macau
N
0 10 20 Km

Fig. 2

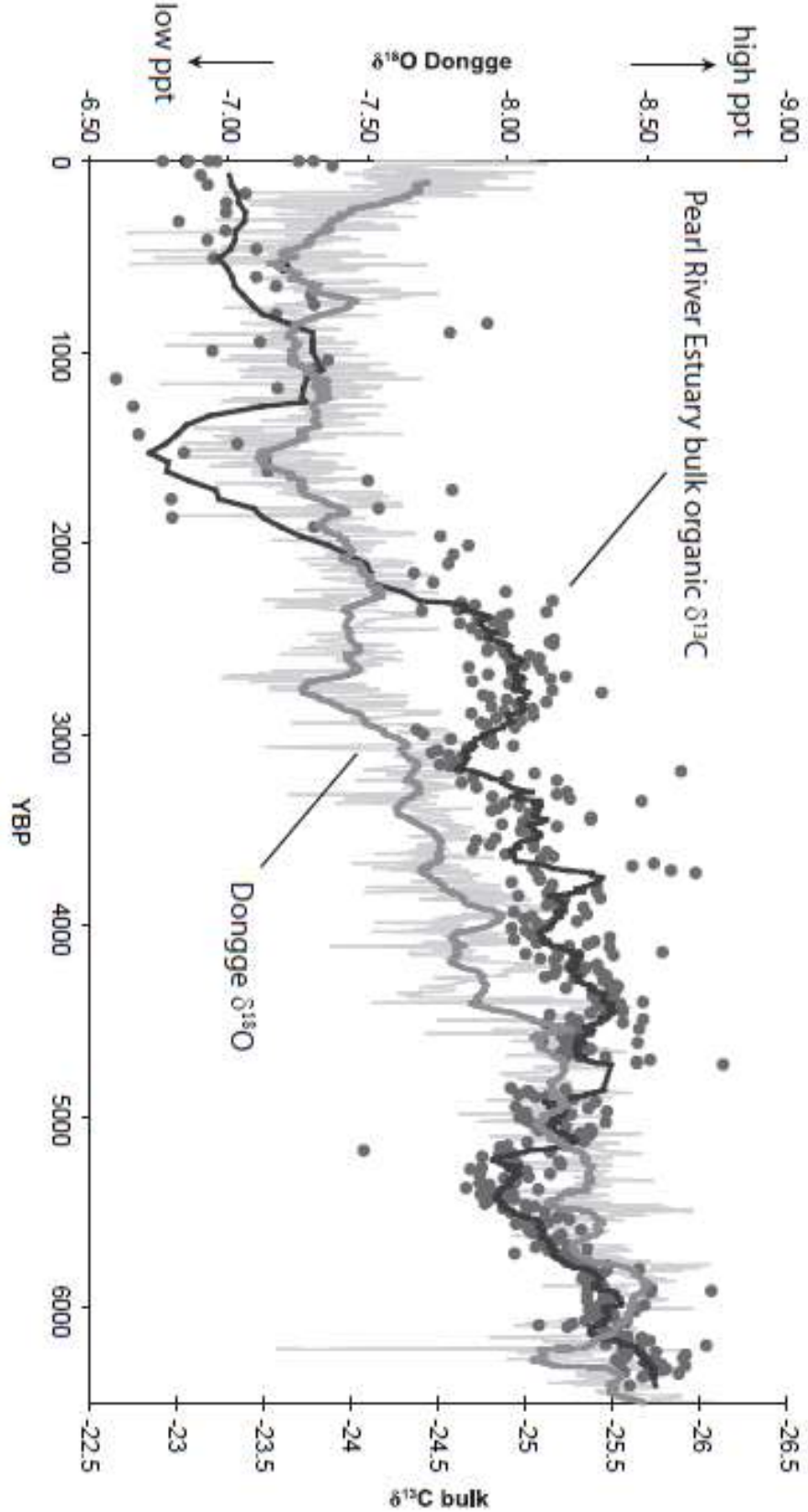
high ppt
low ppt
δ18O Dongge
-9.00
-8.50
-8.00
-7.50
-7.00
-6.50
Pearl River Estuary bulk organic δ13C
Dongge δ18O
0
1000
2000
3000
4000
5000
6000
YBP
-26.5
-26
-25.5
-25
-24.5
-24
-23.5
-23
-22.5
δ13C bulk

Fig. 3

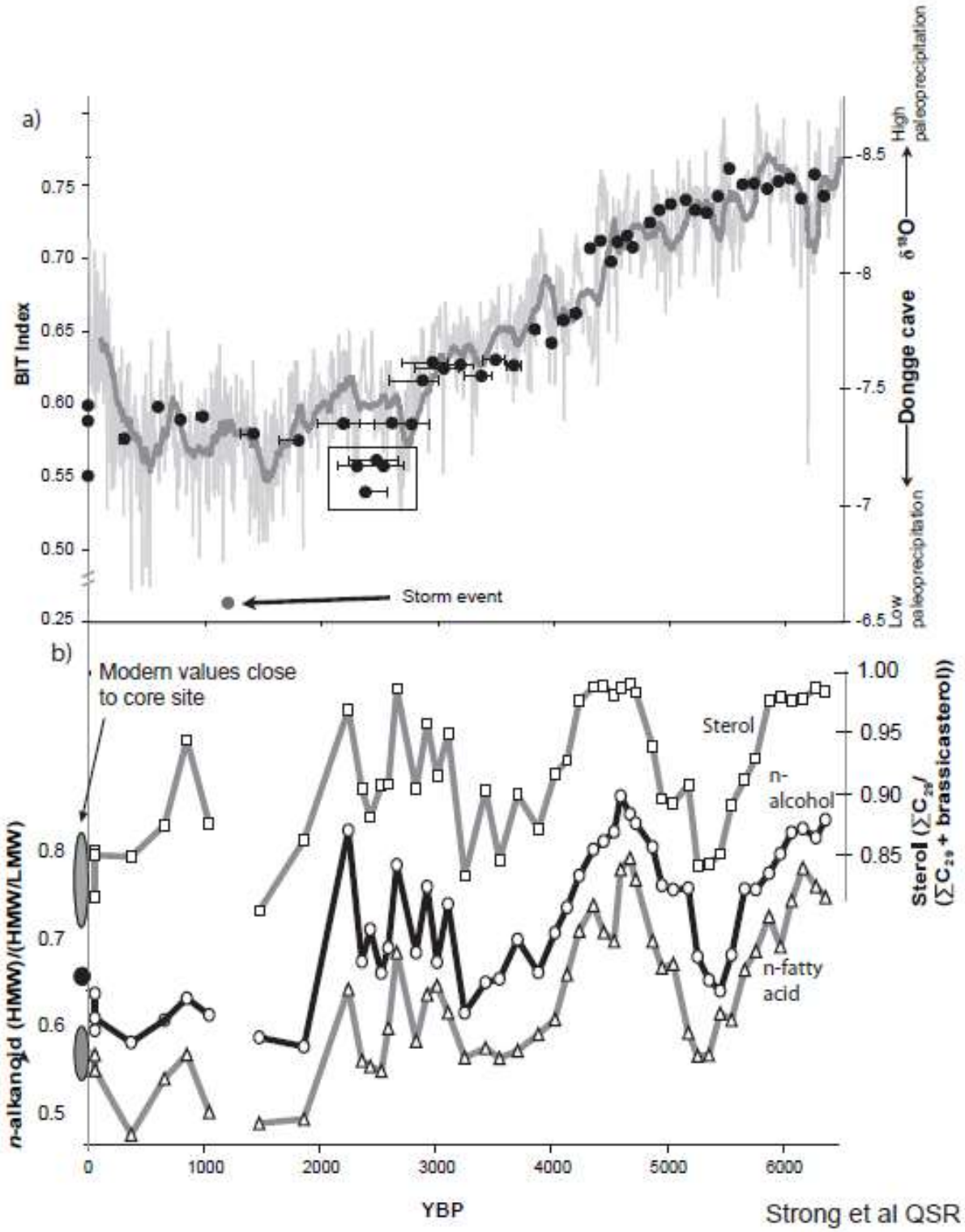
a)
BIT Index
0.75
0.70
0.65
0.60
0.55
0.50
0.25
Storm event
-8.5
-8
-7.5
-7
-6.5
High paleoprecipitation
δ18O
Dongge cave
Low paleoprecipitation
b)
Modern values close to core site
n-alkanol (HMW)/(HMW/LMW)
0.8
0.7
0.6
0.5
Sterol
n-alcohol
n-fatty acid
1.00
0.95
0.90
0.85
Sterol (∑C29/(∑C29 + brassicasterol))
0
1000
2000
3000
4000
5000
6000
YBP
Strong et al QSR

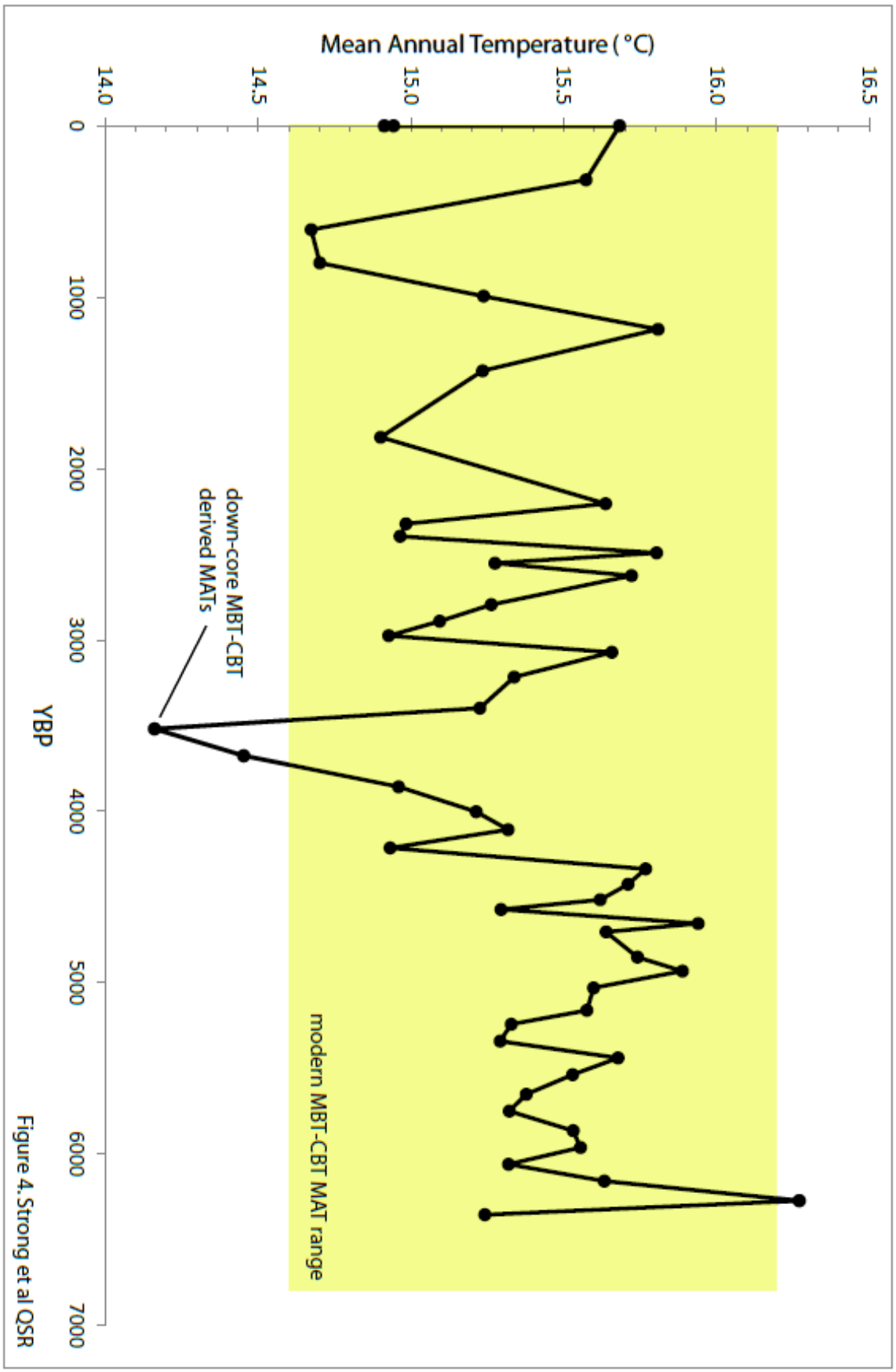

Figure 4. Strong et al QSR

Fig. 5

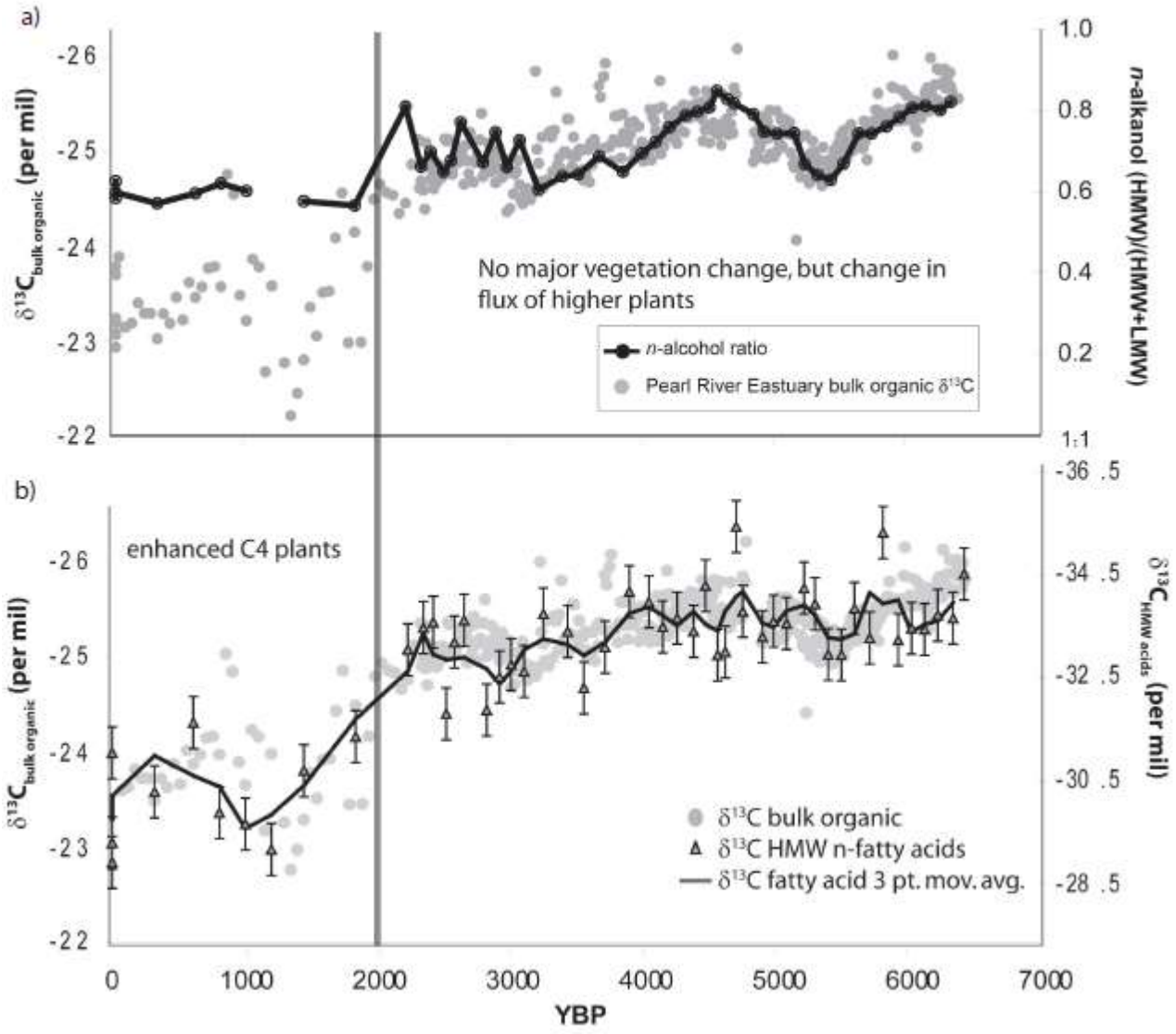
a)
-26
-25
-24
-23
-22
δ13Cbulk organic (per mil)
1.0
0.8
0.6
0.4
0.2
1:1
n-alkanol (HMW)/(HMW+LMW)
No major vegetation change, but change in flux of higher plants
n-alcohol ratio
Pearl River Eastuary bulk organic δ13C
b)
enhanced C4 plants
-36 .5
-34 .5
-32 .5
-30 .5
-28 .5
δ13CHMW acids (per mil)
δ13C bulk organic
δ13C HMW n-fatty acids
δ13C fatty acid 3 pt. mov. avg.
0
1000
2000
3000
4000
5000
6000
7000
YBP

Fig. 6

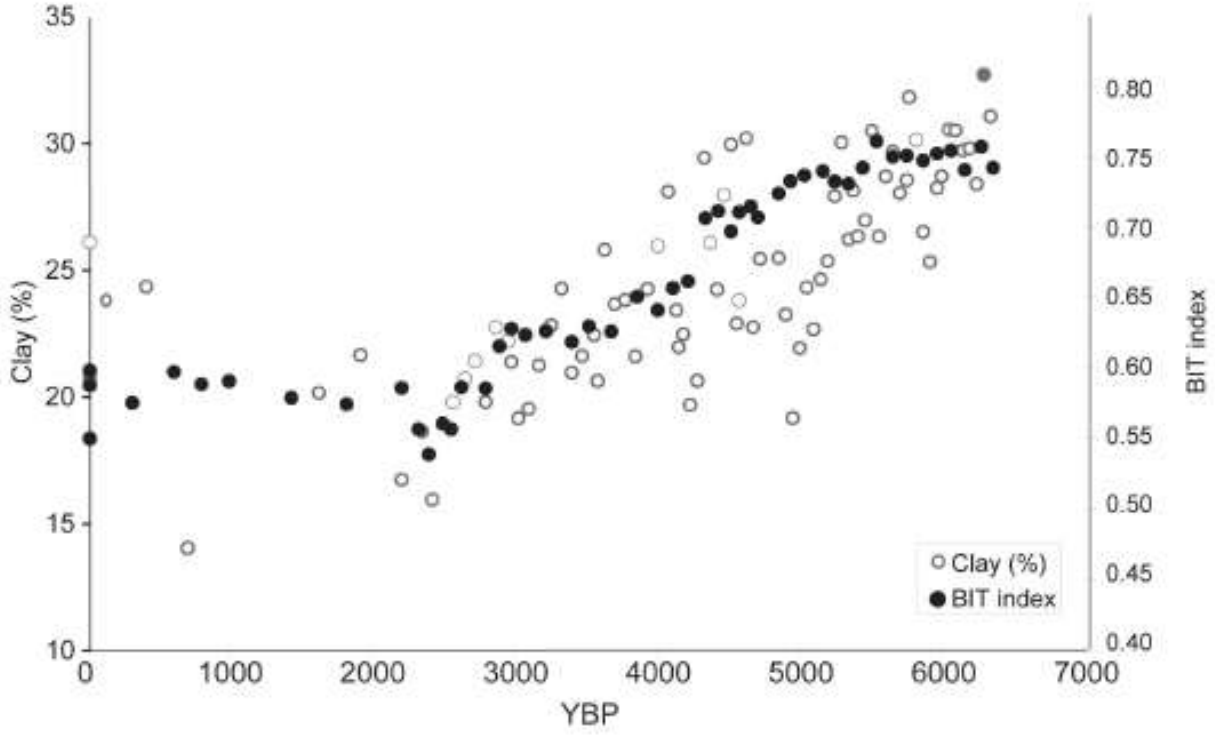
35
30
25
20
15
10
Clay (%)
0.80
0.75
0.70
0.65
0.60
0.55
0.50
0.45
0.40
BIT index
0
1000
2000
3000
4000
5000
6000
7000
YBP
Clay (%)
BIT index

Fig. 7

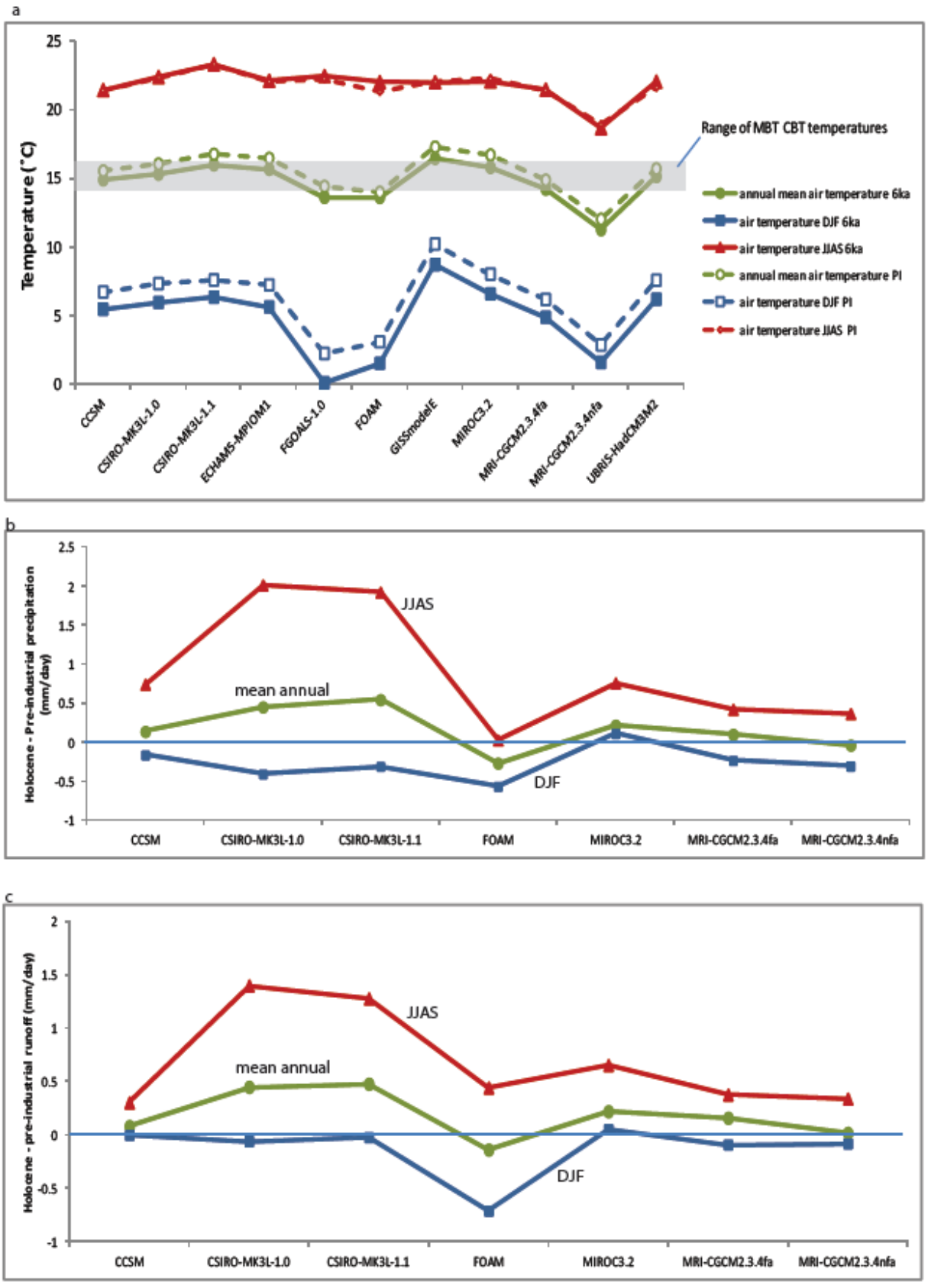
a
Temperature (°C)
25
20
15
10
5
0
Range of MBT CBT temperatures
annual mean air temperature 6ka
air temperature DJF 6ka
air temperature JJAS 6ka
annual mean air temperature PI
air temperature DJF PI
air temperature JJAS PI
CCSM
CSIRO-MK3L-1.0
CSIRO-MK3L-1.1
ECHAM5-MPIOM1
FGOALS-1.0
FOAM
GISSmodelE
MIROC3.2
MRI-CGCM2.3.4fa
MRI-CGCM2.3.4nfa
UBRIS-HadCM3M2
b
Holocene - Pre-industrial precipitation (mm/day)
2.5
2
1.5
1
0.5
0
-0.5
-1
JJAS
mean annual
DJF
CCSM
CSIRO-MK3L-1.0
CSIRO-MK3L-1.1
FOAM
MIROC3.2
MRI-CGCM2.3.4fa
MRI-CGCM2.3.4nfa
c
Holocene - pre-industrial runoff (mm/day)
2
1.5
1
0.5
0
-0.5
-1
JJAS
mean annual
DJF
CCSM
CSIRO-MK3L-1.0
CSIRO-MK3L-1.1
FOAM
MIROC3.2
MRI-CGCM2.3.4fa
MRI-CGCM2.3.4nfa